Leveling and Dewetting Processes of Nanoindentation-Induced Defects on Thin Polymer Films

Ioannis Karapanagiotis, D. Fennell Evans, and William W. Gerberich*

Department of Chemical Engineering and Materials Science, University of Minnesota, Minneapolis, Minnesota 55455

Received October 11, 2000; Revised Manuscript Received January 23, 2001

ABSTRACT: We study the effect of nanoindentation-induced indents on polystyrene (PS) films (thickness $= h >$ 100 nm), spin-cast on silicon substrates. Indents with residual depths of penetration, z_D, comparable to the film thicknesses leveled (healed) upon heating above the glass transition temperature (T_g) of bulk PS, resulting in a flat polymer surface. Deep indents which clearly penetrated the films and damaged the substrate dewetted from the silicon surface. The healing rate, dz_D/dt, was measured for several molecular weight PS films and found to scale with the curvature of the hole bottom, H_D, as $(dz_D/dt) \sim H_D^{0.52\pm0.05}$. Measurements were performed using atomic force microscopy. The healing rate was found to be, in general, higher than the dewetting rate of the laterally expanded deep indents.

1. Introduction

Thin polymer films placed on hard substrates have received significant attention due to their applications in the microelectronics industry, printing technology, and other areas that use plastic coatings as decorative and protective surface covers, as well as lubricant layers. Usually these applications require smooth and defect-free polymer coatings. However, when these films are placed on nonwettable surfaces, they can develop dry patches (nucleation sites) that expose substrate area to the air.[1−5] The spontaneous formation of the nucleation sites for dewetting onset is the result of the competition of two interactions:[1,5,6] (i) the repulsive van der Waals interaction between the polymer film and the nonwettable substrate, which amplifies surface disturbances until tiny dry patches are formed, and (ii) the Laplace pressure which tends to level the film. In the dewetting phenomenon the former overcomes the latter. Other studies have suggested that dewetting is initiated by intrinsic film defects.[7] For the system that we study, polystyrene (PS) films spin-cast on silicon (Si) surfaces, disturbances have been identified as indents that grow toward the substrate, upon heating above the glass transition temperature of PS.[6] Once dry patches form, they grow laterally until the polymer mass is accumulated in arrays of droplets that form connected polygons. In this study we focus on PS coatings sufficiently thick (film thickness $= h >$ 100 nm) to prevent spontaneous dewetting. In these films dewetting can be initiated by dry patches, formed by extrinsic defects (e.g., particles[6] or nanoindentation induced defects[8]), when their geometrical conformation is such that a critical excess surface energy barrier is exceeded.[8] If the energetic barrier is not exceeded, the dry patches "close", resulting in a flat film surface.[8]

A nanoindentation device was used to induce indents (surface disturbances) on PS coatings at room temperature. Large indents, imposed under high forces, clearly penetrated the films and damaged the Si substrate. In this case the residual depth of penetration, z_D, of the indents was higher than the film thickness, h, $z_D > h$. These indents grew laterally, exposing more Si surface to the air upon heating above the T_g of bulk PS. The lateral growth process was monitored using an atomic force microscope (AFM), and the standard dewetting kinetic laws[9−11] were verified. Small indents, imposed under low forces, corresponded to penetration depths, z_D, that were equal to or less than the film thicknesses, h, $z_D \leq h$. Instead of growing, these indents leveled (healed), resulting in a flat polymer surface. The leveling process of a disturbance induced at the free surface of a film has been extensively studied mainly by numerical procedures.[12,13] Using AFM, the dynamics of the leveling process of PS films was recorded on an experimental basis.

Table 1. PS Properties: Bulk Glass Transition Temperatures, T_g,[14] and Bulk Viscosity, η, Values for 110 and 140 °C[15,16]

			$\eta/10^5$ (P)	
M_w(g/mol)	M_w/M_n	T_g (°C)	for 110 °C	for 140 °C
13 700	1.06	93	1100	0.5
18 700	1.07	95	3400	1.0
29 300	1.09	97	13500	3.0
44 000	1.08	98	48500	8.0
114 200	1.08	99	2×10^6	250
212 400	1.11	100	2.3×10^7	2550

In the following we first describe the experimental procedure that was followed. We then describe the leveling process of small indents. The healing or leveling rate of the thin regions (holes) of the induced surface disturbances is measured for different molecular weight PS as a function of the local mean curvature. Dewetting measurements are then presented briefly. Finally we compare the leveling process with the lateral growth process on a kinetic basis; that is, we compare the healing rate with the dewetting rate.

2. Experimental Section

Standardized PS (Aldrich Chemical Co., Milwaukee, WI) with various molecular weights was dissolved in spectroscopic grade toluene to produce 5 wt % solutions. Table 1 shows the molecular weights of the PS samples and the corresponding bulk glass transition temperature (T_g) and viscosity values.[14−16] Si wafers (Virginia Semiconductor, Fredericksburg, VI) were spin-coated with the solutions. To remove residual solvent, the coatings were then annealed at 90 °C overnight. The thickness range of the resulting films was determined by ellipsometry and found to be 100−150 nm, depending on the molecular

10.1021/ma001762h CCC: $20.00
Published on Web 04/20/2001

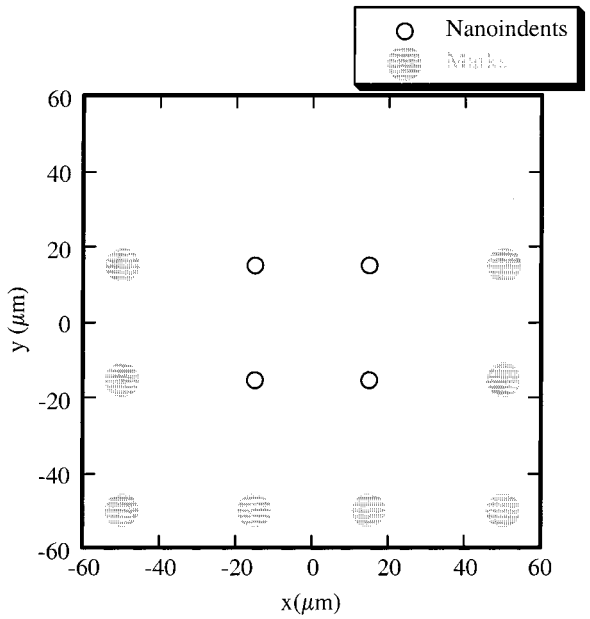

Figure 1. Nanoindentation pattern used to study the leveling process of nanoindents. Big indents (marks) were visible with an optical microscope. Nanoindents were revealed by scanning with AFM.

weight and spinning rate. Spin-coating was performed in a clean room (class 10) to minimize particle contamination of the films. The ⟨100⟩ oriented Si wafers were tested with ellipsometry, prior to spin-coating, to reveal the presence of a 1.7 nm thick native oxide film.

Using a nanoindentation Hysitron triboscope (Hysitron Inc., Minneapolis, MN) apparatus, a series of indents were induced on each coating. The nanoindentation device adapts to an AFM which utilizes a Hysitron microsensor system, instead of the standard AFM head component, for applying loads electrostatically. A standard three-sided pyramid (Berkovich) diamond tip of nominal radius 300 nm was used for the indentations. The indentation pattern is shown in Figure 1. Nanoindents were induced using forces within a range of 230−270 μN. Big indents (marks) imposed under high forces (11 mN) served as markers to locate the indentation area with an optical microscope.

After the indentation, residual indents were scanned with a Nanoscope III SPM (Digital Instruments, Santa Barbara, CA) operated in the contact mode. During the image acquisition, forces in the range of 1−10 nN were applied from the 200 μm cantilever to the polymer surface. Repeated scanning of the same polymer area showed no alteration of the surface topography due to the interaction force between the polymer and the cantilever. AFM images after indentation showed that the depths of the nanoindents were less than or approximately equal to the corresponding film thicknesses. The evolution of the imposed indents (leveling process) upon heating at 110 °C was then recorded by AFM, following a cyclic procedure of heating−imaging at room temperature, meaning that the samples had to be quenched for each image acquisition.

In the same set of samples, large indents were induced under a force range of 2−4 mN. The lateral growth of the imposed indents (dewetting process), upon heating at 140 °C, was then recorded by AFM, following the cyclic procedure of heating−imaging at room temperature.

3. Results and Discussion

Leveling Process. Figure 2 shows AFM images of a small indent induced by nanoindentation at room temperature (Figure 2a) and after heating the system above the T_g of PS (Figure 2b). Initially, the indent is triangular because a three-sided pyramid (Berkovich) tip was used for the nanoindentation test. Upon heating, the top view shape of the indent evolves to circular. Using such AFM images for several indents, we monitored the evolution process shown schematically in Figure 3. The vertexes of the initial triangle become round as they move slightly to the center of the forming circle. The sides of the triangle become round as they move outward. The process continues until the indent becomes circular, and it is followed by a subsequent lateral "expansion" of the circle, resulting in an increase of radius R (R is defined in Figure 4).

Figure 4 shows the cross-sectional evolution (leveling process) of an indent with time, t. Cross sections were extracted from the corresponding AFM images. Upon heating above T_g, the indent depth, z_D, decreases and finally becomes zero, corresponding to a flat polymer surface. The height of the surrounding rim, z_R, decreases as well. The radius, R, of the indent, defined at the level of the flat-free surface, increases and so does the width, w, of the rim. Therefore, during the leveling process the indent "contracts" in the vertical, z, direction and "expands" in the lateral, x, direction until it becomes flat and not distinguishable from the rest of the polymer surface. One can describe the leveling process, shown in Figure 4, as the result of two processes that interplay: (i) the healing process of the hole bottom that

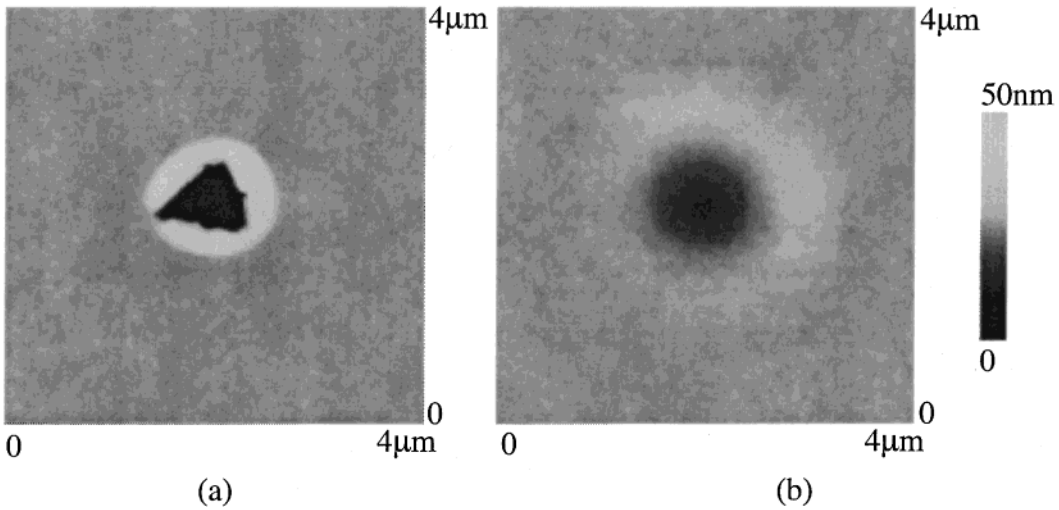

Figure 2. AFM images of a nanoindent right after indentation (a) and after heating at 110 °C for 8.5 min (b). The molecular weight of PS was M_w = 13 700 g/mol. The nanoindent (a) was induced by a 270 μN force.

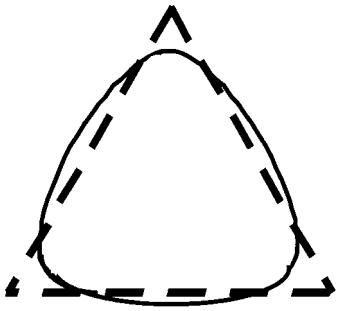

Figure 3. Schematic illustration of the top view indent evolution upon heating above T_g. The sides and vertexes of the initial triangular indent (dashed line) become round (solid line) to result in a circle (shown in Figure 2b).

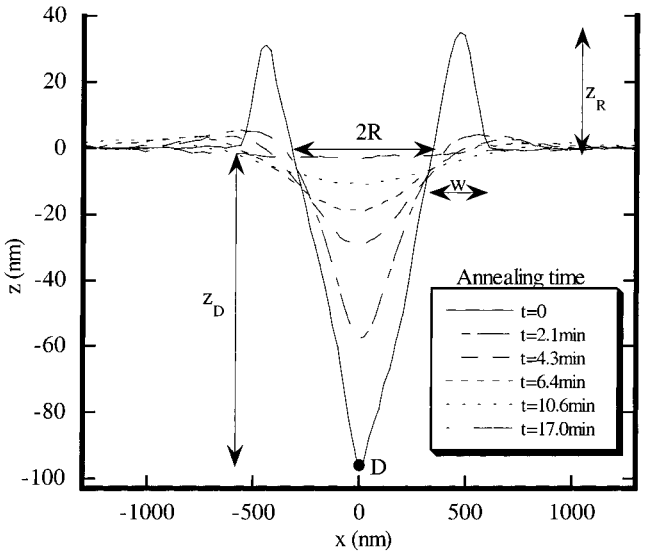

Figure 4. AFM cross sections of an indent at several annealing times ($T = 110$ °C). The indent depth, z_D, rim height, z_R, indent radius, R, and rim width, w, are shown for the cross section that corresponds to $t = 0$ (right after indentation and prior to any thermal treatment above T_g). Point D corresponds to the maximum indent depth, z_D, and it is shown for $t = 0$. The film thickness was 100 nm, and the molecular weight was $M_w = 13\,700$ g/mol.

results in the decrease of the indent depth, z_D, and (ii) the relaxation process of the surrounding rim that results in the decrease of the rim height, z_R. Figure 4 suggests that the rim relaxation is faster than the hole healing process; i.e., the rim height, z_R, decreases faster to a very small value and then to zero, compared to the hole depth, z_D. This is in accordance with theoretical studies associated with the leveling dynamics of a wave developed at the free surface of film. A finite element analysis has suggested that the leveling process of a sinusoidally disturbed film is faster in the thick regions than in the thin ones.[12,13] Although the cross-sectional profiles of the indents differ substantially from a sinusoidal perturbation, the numerical prediction coincides with our experimental observation. Rims (thick regions) level faster than the corresponding holes (thin regions).

Figure 5a shows the decrease of indent depth, z_D, as a function of annealing time, t, for PS coatings corresponding to molecular weights, M, lower than the critical entanglement molecular weight, M_c, $M < M_c$. Figure 5b includes measurements for PS coatings with $M > M_c$. For PS the critical entanglement molecular weight is $M_c = 38\,000$ g/mol.[15] The initial depths, at $t = 0$, of the six indents of Figure 5 ranged from 96 to

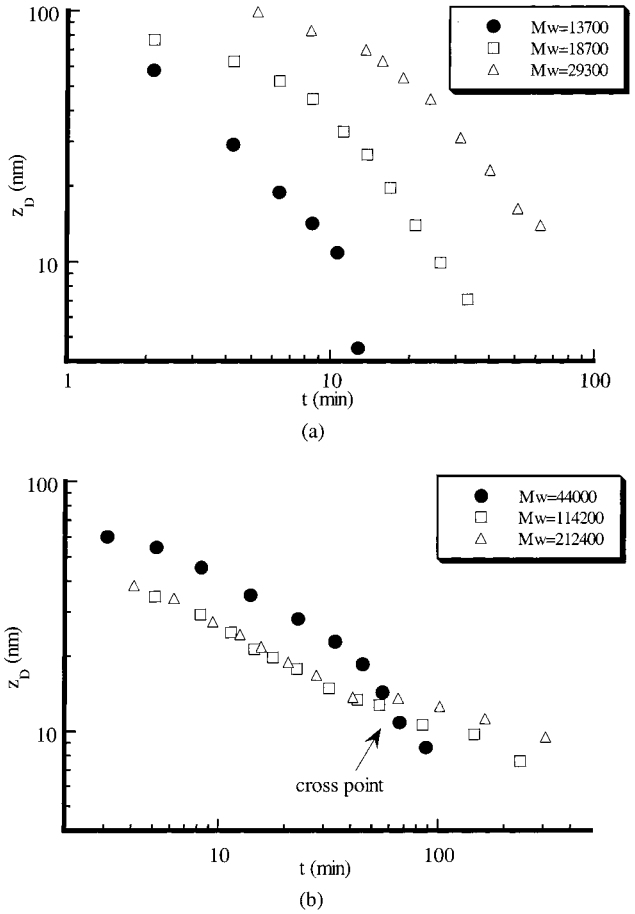

Figure 5. Indent depths, z_D, as a function of annealing time, t, for films with $M < M_c$ (a) and $M > M_c$ (b). Data correspond to 110 °C.

103 nm (not shown here) with the lowest corresponding to $M_w = 18\,700$ g/mol and the highest to $M_w = 212\,400$ g/mol. The depth range of the initial indents does not affect the trend of the data which was verified by other sets of measurements corresponding to different initial depth ranges. The indents were then heated at 110 °C to level the surface. Figure 5a provides the expected result: the higher the molecular weight, the higher the hole depth, z_D, at a particular annealing time, meaning that the absolute value of the healing rate, $|dz_D/dt|$, decreases with the molecular weight, M. In Figure 5b the results become more complicated. For $z_D > 15$ nm the indents induced on high molecular weight samples ($M_w = 114\,200$ g/mol and $M_w = 212\,400$ g/mol) correspond to similar z_D values at a particular annealing time, and the indent imposed on PS with $M_w = 44\,000$ g/mol corresponds to higher z_D. When the indents become very shallow, $z_D < 15$ nm, the expected behavior observed in Figure 5a is restored. Several similar measurements for indents with $M > M_c$ showed the same behavior. In the following we provide a possible explanation for this behavior.

The surface disturbances that we study were induced by nanoindentation at room temperature. The indentation technique results in the formation of a stress field around a residual indent. These stresses relax upon heating at 110 °C, which is the temperature that the leveling process was recorded. One can expect that the relaxation of the stresses, induced upon nanoindentation, should affect the leveling process and therefore the healing rate, dz_D/dt. The importance of the stress field

is determined by the value of the elastic Young's modulus, E. At 110 °C entangled PS has a higher E than low molecular weight PS ($M < M_c$) for two reasons: (i) the presence of the rubbery plateau existing for $M > M_c$ provides a higher value of E, and (ii) the glass transition temperature, T_g, for $M > M_c$ is closer to the annealing temperature of 110 °C, which was used to heat the coatings, than the T_g for $M < M_c$ (Table 1). Consequently, the magnitude of the stresses, induced upon nanoindentation, that the indent bottom experiences at 110 °C should be considerable higher for entangled PS ($M > M_c$) than for low molecular weight PS ($M < M_c$). Therefore, an augmented role of the stress field, induced by the indenter, in the hole healing process should be expected for PS with $M > M_c$. For PS with $M < M_c$ the low residual stresses should relax fast, and the leveling process should be driven mainly by the existing curvature at the indent bottom which must be reduced to minimize the Laplace pressure; i.e., the indent must become flat. In this case the healing rate, dz_D/dt, should be determined by the mobility of the polymer chains or i.e. the viscosity of the polymer as is shown in Figure 5a: the higher the molecular weight, the lower the $|dz_D/dt|$. For PS with $M > M_c$ the high residual stresses should affect the healing process for a longer time period. For higher molecular weight PS, the magnitude of the stresses should be higher, and their effect in the healing process should be more pronounced. Even in this case, however, continuous annealing at 110 °C will result at some point in the relaxation of the residual stresses. After this the hole healing process will be driven mainly by the indent curvature in the same way as in Figure 5a. Therefore, after the cross point, shown in Figure 5b for late annealing time stages, indents induced into high molecular weight PS samples correspond to higher z_D values.

The maximum residual stress induced upon nanoindentation can be estimated as $\sim^1/_2 E\epsilon$, where E is the elastic Young's modulus and ϵ is the strain.[17] For PS at 110 °C the typical magnitude of E is ~2 MPa.[18] For a three-sided (Berkovich) indenter tip the induced strain is equal to $\epsilon = \tan\theta$, where $\theta = 19.7°$ is the angle that the faces of the tip make with respect to the top surface. The maximum residual stress is then estimated to be ~0.36 MPa. This value corresponds to the maximum stress present initially ($t = 0$) at the vicinity of an indent, heated at 110 °C. With heating time this value reduces. We note also that $E \sim 2$ MPa corresponds to high molecular weight, entangled PS. For PS with $M < M_c$ one can expect a lower modulus, E, and therefore a lower value for the stress. An order of magnitude difference on the E (and therefore stress) values between PS samples with $M \sim 10^4$ and $M \sim 10^5$ at 110 °C (Figure 5) can be considered as possible. The difference might be more pronounced if instead of using the E of bulk PS to estimate the maximum stress, we used the corresponding surface modulus values. It has been reported[19] that at room temperature an order of magnitude difference in the surface dynamic storage (E') moduli of unentangled and entangled PS samples exists. One might expect a similar (if not higher) difference at elevated temperatures.

The approach presented above might overestimate the residual stress as it is based on an elastic analysis. For small indentation depths, also applicable to the properties of thin films, the measured yield strength for poly(methyl methacrylate) (PMMA) is 150−200 MPa, approximately 3−4 times the bulk yield strength.[20] A similar value is expected for PS. Assuming yield point residual stresses around the indentation with the elevated yield stress in thin PS films, the room-temperature residual stress is estimated to be 150−200 MPa. If we then scale the room-temperature yield stress with the ratio of bulk moduli (2 MPa/3 GPa), the residual stress is calculated to be 0.1−0.13 MPa at 110 °C. This is smaller than the value of 0.36 MPa calculated from the elastic analysis, but it is of the same order of magnitude. Also, it refers to high molecular weight ($M > M_c$) PS. For PS with $M < M_c$ a lower yield strength, and consequently a lower residual stress is expected.

Our next goal is to characterize the indents on a geometrical basis: that is to calculate their curvatures. Curvature values will be used later to interpret the dynamics of the hole healing process. In 2D the curvature of a curve, described by a function $y = f(x)$, at a given point $A_0(x_0,y_0)$ is defined as

$$K_{A_0} = \frac{|f''(x_0)|}{[1 + f'(x_0)^2]^{3/2}} \tag{1}$$

The radius of curvature at a point A_0, R_{A_0}, is defined as $R_{A_0} = 1/K_{A_0}$. In 3D the mean curvature of a surface at point A_0 is given by

$$H_{A_0} = \frac{1}{2}(K_{1A_0} + K_{2A_0}) \tag{2}$$

where K_{1A_0} and K_{2A_0} are the maximal and minimal values of the curvature K_{A_0} of a section normal to the surface at point A_0. For an indent the value of the mean curvature H_{A_0} depends on the position of point A_0. In the following we focus on point D (Figure 4), which corresponds to the maximum indent depth z_D. The choice of point D is based on three reasons: (i) Point D is expected to correspond to the highest mean curvature, H_D. Therefore, any effect from the curvature reduction, during the healing process, should be more pronounced at this point. (ii) It has been mentioned that during the healing process an indent "contracts" in the perpendicular direction and "expands" laterally. Consequently, the motion of any point at the surface of the indent (except point D) is the result of two components: a lateral and a vertical motion. Point D is the only one which moves only along the vertical, z, direction. Therefore, focusing on point D simplifies the dynamics of the healing process, since it "eliminates" the effects of the lateral motion. (iii) The measurement of the mean curvature at any point of the indent is a difficult problem. On the contrary, the mean curvature of point D can be measured relatively easy. Figure 6 shows schematically the indent bottom and the radii of curvature R_1 and R_2 for point D and for another random point E at the indent surface. In both cases R_1 and R_2 are orthogonal. For point D, R_1 is the radius of curvature of segment D_1DD_2 which lies on the plane of the page. R_2 is the radius of curvature of segment D_3DD_4 which is contained in the plane that is perpendicular to the page. R_1 and R_2 can be easily measured from AFM images. For the random point E, R_1 is the radius of curvature of segment E_1EE_2 which lies on the plane of the page and R_2 is the radius of curvature of segment E_3EE_4 which is contained in the plane that is perpendicular to the page. Although R_1 can be easily measured,

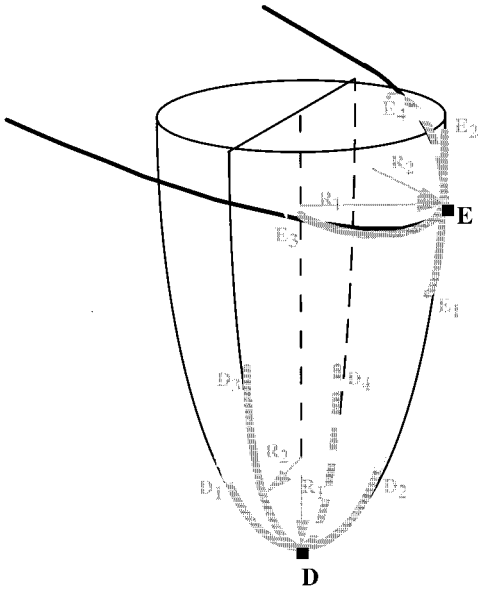

Figure 6. Schematic illustration of indent bottom. Point D corresponds to the maximum indent depth, z_D, and point E is a random point. The 2-dimensional orthogonal radii of curvature R_1 and R_2 are shown for both points.

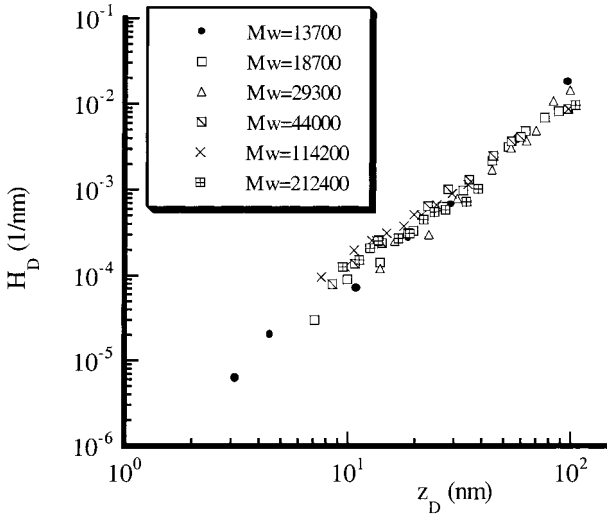

Figure 7. Curvature of indent bottom, H_D, vs indent depth, z_D. Measurements for six molecular weights (Table 1) are shown. Data correspond to 110 °C.

R_2 requires a reliable 3-dimensional analysis of the indent bottom to determine the coordinates of the segment E_3EE_4.

To measure the curvature at point D, we took several cross sections of the indent bottoms (e.g., segments like D_1DD_2 in Figure 6) and described them by fourth-order polynomial functions, $y = f(x)$. Then we calculated K_D values for several directions (e.g., D_1DD_2 and D_3DD_4 in Figure 6) using eq 1. Then, using eq 2, we took a mean value of the lowest and highest K_D values. Figure 7 shows the change of indent curvatures, H_D, with the corresponding indent depths, for six indents induced on different molecular weight PS coatings (Table 1). During the healing process the hole depth, z_D, decrease is accompanied by a curvature, H_D, decrease. In 2 dimensions, this is also obvious in Figure 4. The six indents of Figure 7 were induced using the same Berkovich tip, and therefore the initial H_D corresponding at maximum z_D has similar values in all six cases. The initial depths of the indents were lower than the corresponding film

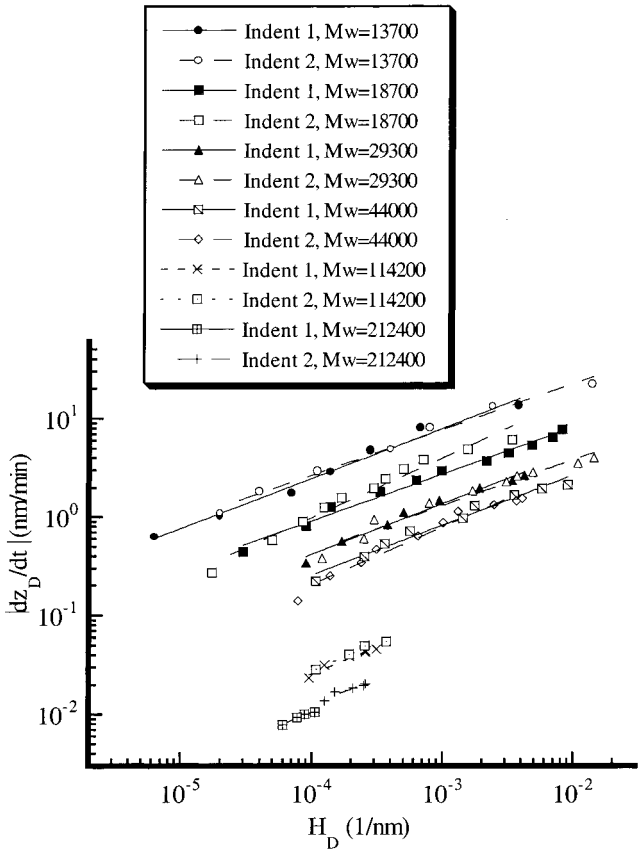

Figure 8. Absolute value of the hole healing rate, $|dz_D/dt|$, vs curvature of indent bottom, H_D. Measurements for two healing indents for each molecular weight (Table 1) are shown. Power law curve fits are also shown, and the equations are displayed in Table 2. Data correspond to 110 °C.

thicknesses, $z_D < h$. Figure 7 suggests also that the curvature−depth relation of a healing indent is independent of the molecular weight of the film on which the indent is induced.

Having curvature values the Laplace pressure can be calculated as $2\gamma H$,[21] where γ is the surface energy of PS and H the curvature. Using the data of Figure 7, an augmented Laplace pressure can be estimated, as point D is expected to correspond to high curvature values. Initially at $z_D = 10^2$ nm the curvature is $H_D \sim 10^{-2}$ nm^{-1}. For PS with $M \sim 10^5$ at 110 °C, $\gamma = 34.7$ mN/m.[14] This results in a Laplace pressure of 0.7 MPa. A similar value can be estimated for low molecular weight PS ($M \sim 10^4$) as the initial H_D is approximately the same for all samples and γ exhibits a very weak molecular weight dependence. We note here that the calculated initial augmented Laplace pressure (0.7 MPa) is comparable to the initial maximum stress, estimated for high molecular weight ($M \sim 10^5$) PS samples, which was estimated to be 0.1−0.36 MPa. This comparison provides evidence that at short annealing times the stress field around an indent induced on high molecular weight PS sample can play an important role in the healing process. As was mentioned before, the reduced elastic modulus and/or the reduced yield strength of PS samples with $M < M_c$ results in lower stresses. In this case the Laplace pressure dominates.

In Figure 8 we plot in a log−log scale the absolute value of the healing rate, $|dz_D/dt|$, as a function of the corresponding curvature H_D for the samples of Table 1. For each sample data for two healing indents are

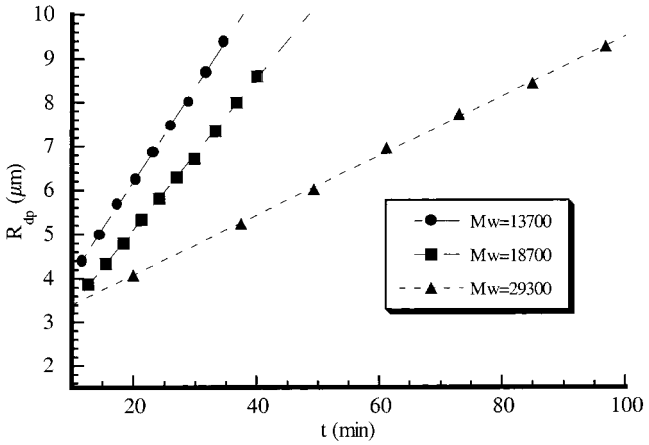

Figure 9. Radius of dry patch, R_{dp}, vs time, t. Measurements for three molecular weights are shown. Data correspond to 140 °C.

Table 2. Power Law Curve Fits from Figure 8

$M_w = 13\,700$	indent 1	$y = 268.25x^{0.51}$
	indent 2	$y = 190.03x^{0.46}$
$M_w = 18\,700$	indent 1	$y = 72.73x^{0.48}$
	indent 2	$y = 264.11x^{0.61}$
$M_w = 29\,300$	indent 1	$y = 47.45x^{0.51}$
	indent 2	$y = 32.78x^{0.47}$
$M_w = 44\,000$	indent 1	$y = 27.58x^{0.51}$
	indent 2	$y = 44.48x^{0.58}$
$M_w = 114\,200$	indent 1	$y = 3.91x^{0.55}$
	indent 2	$y = 4.39x^{0.55}$
$M_w = 212\,400$	indent 1	$y = 1.46x^{0.54}$
	indent 2	$y = 1.04x^{0.48}$

provided. The data are power law fit with power indices provided in Table 2. Table 2 suggests that the healing rate scales with the curvature as

$$\frac{dz_D}{dt} \sim H_D^{0.52\pm0.05} \tag{3}$$

We note here that this conclusion is based on isothermal measurements ($T = 110$ °C), and it is independent of the molecular weight of the film. Healing rates, dz_D/dt, were calculated from plots like those in Figure 5, by fitting the data with $z_D = 10^{\alpha t+\beta}$. Since the depth values were taken as positive numbers (Figures 4 and 5) the healing rate, dz_D/dt, is defined as a negative quantity. To eliminate the negative sign in Figure 8, we plot the absolute value of the healing rate. Finally, we note that for the very high molecular weight samples ($M_w =$ 114 200 g/mol and $M_w = 212\,400$ g/mol) we disregarded the initial time stages, and we included data that corresponded only to the late annealing time stages, i.e., data for $z_D < 15$ nm in Figure 5b. For these samples with $M \gg M_c$ if we consider the initial data points for $z_D > 15$ nm, deviations from eq 3 are observed, indicating that an additional mechanism, apart from the curvature (or Laplace pressure) reduction, must be considered. Previously, we provided arguments showing that the stress effect cannot be neglected for high molecular weight samples. All the data points for the rest of the PS samples were included in Figure 8, except points that correspond to $t = 0$.

Dewetting Process: Comparison. Industrially, dewetting is usually an undesirable process as it results in a discontinuous film. On the contrary, leveling eliminates defects that disrupt the film. Consequently, a kinetic comparison of the leveling with the dewetting

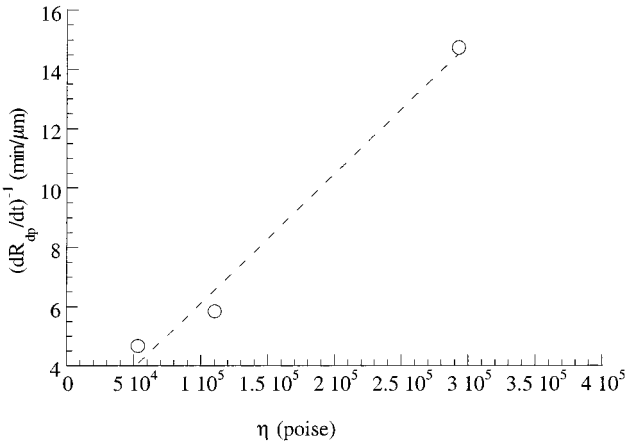

Figure 10. Inverse of dewetting rate, $(dR_{dp}/dt)^{-1}$, vs viscosity, η. Measurements for the three molecular weights of Figure 9 are presented. Data correspond to 140 °C.

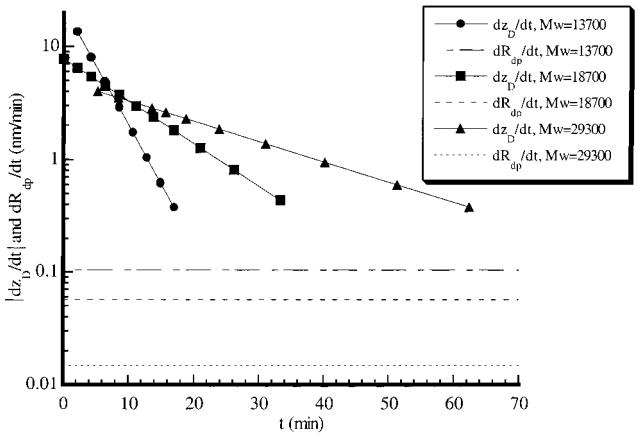

Figure 11. Absolute value of healing rate.

rate might be of interest. Dewetting rates were measured for the three lowest molecular weight ($M < M_c$) samples of Table 1, by inducing deep indents that clearly penetrated the films and damaged the substrate. As in the leveling process, the initial indents were triangular, because a three-sided pyramid was used for the nanoindentation. The triangular indents evolved to circular dry patches during the dewetting process. Figure 9 shows the radii of the developed circular dry patches, R_{dp}, vs time. The expected linear behavior,[9] $R_{dp} \sim t$, is verified from which the dewetting rate, dR_{dp}/dt, can be calculated for each molecular weight. To compare $|dz_D/dt|$ with dR_{dp}/dt, we have to convert the dewetting rates measured at 140 °C to corresponding values for 110 °C, which was the temperature used to study the leveling process. It is well-known that[9]

$$\frac{dR_{dp}}{dt} \sim \frac{\gamma}{\eta}\theta_e^3 \tag{4}$$

where γ and η are the surface tension and the bulk viscosity of the dewetting film and θ_e is the equilibrium contact angle. The surface tension, γ, and the contact angle, θ_e, have a very weak dependence on the molecular weight.[11] Consequently, eq 4 is reduced to $(dR_{dp}/dt) \sim 1/\eta$, which is verified in Figure 10. Viscosity values are shown in Table 1. Having viscosity values (Table 1) and dewetting rate measurements for 140 °C, the corresponding dewetting rate values for 110 °C were calculated and compared to the corresponding healing rates,

$|dz_D/dt|$, in Figure 11 for samples with $M < M_c$. While the dewetting rate for a particular molecular weight, M, is constant with time, the healing rate decreases (on absolute value). The dewetting is lower than the healing rate except after long annealing times, at which the healing rate approaches to zero. This "cross" point is not shown in Figure 11, but it can be predicted by following the trend of the healing rate, $|dz_D/dt|$, data.

4. Conclusions

Kinetic measurements associated with the evolution of nanoindentation-induced defects on thin PS films on Si, upon heating above T_g, are presented. Small indents with depths of penetration, z_D, comparable to the film thicknesses ($z_D \leq h$), were leveled (healed), resulting in a flat polymer surface. Thin regions (holes) were found to heal faster than thick regions (rims). The vertical leveling process of an indent was accompanied by a simultaneous lateral shape change: the initial triangular indent evolved to a circle with increasing radius. Measurements for PS films with different molecular weights showed that the healing rate, dz_D/dt, depends on the curvature as, $(dz_D/dt) \sim H_D^{0.52\pm0.05}$, with D being the point at the bottom of the indent. Apart from the curvature, healing rate may also be affected by the stress field relaxation, induced upon nanoindentation. The latter has been speculated to have an appreciable effect at the initial annealing time stages for high molecular weight ($M \gg M_c$) PS films. In this case, the healing rate was found to follow the proportionally $(dz_D/dt) \sim H_D^{0.52\pm0.05}$ at later annealing time stages, indicating that with sufficient time at temperature the residual stresses have been removed. Large indents clearly penetrated the films ($z_D \gg h$) and grew laterally, i.e., dewetted from the substrate. The radius of the evolving dry patch, R_{dp}, was found to scale linearly with time, $R_{dp} \sim t$. Dewetting rates, dR_{dp}/dt, were compared with corresponding healing rates. In general, $|dz_D/dt| > dR_{dp}/dt$ until the depth of a healing indent becomes very small (indent is almost flat in Figure 4) so that the healing rate approaches to zero. Comparisons were made for PS samples with $M < M_c$.

Acknowledgment. Support by the Center for Interfacial Engineering (CIE), a National Science Foundation Engineering Research Center, is gratefully acknowledged.

References and Notes

(1) Brochard-Wyart, F.; Daillant, J. *Can. J. Phys.* **1990**, *68*, 1084.
(2) Reiter, G. *Phys. Rev. Lett.* **1992**, *68*, 75.
(3) Reiter, G. *Langmuir* **1993**, *9*, 1344.
(4) Reiter, G. *Macromolecules* **1994**, *27*, 3046.
(5) Sharma, A.; Reiter, G. *J. Colloid Interface Sci.* **1996**, *178*, 383.
(6) Stange, T. G.; Hendrickson, W. A.; Evans, D. F. *Langmuir* **1997**, *13*, 4459.
(7) Jacobs, K.; Mecke, K. R.; Herminghaus, S. *Langmuir* **1998**, *14*, 965.
(8) Karapanagiotis, I.; Gerberich, W. W.; Evans, D. F., submitted to *Langmuir*.
(9) Redon, C.; Brochard-Wyart, F.; Rondelez, F. *Phys. Rev. Lett.* **1991**, *66*, 715.
(10) Redon, C.; Brzoska, J. B.; Brochard-Wyart, F. *Macromolecules* **1994**, *27*, 468.
(11) Stange, T. G. Ph.D. Thesis, University of Minnesota, 1997.
(12) Kheshgi, H. S. Ph.D. Thesis, University of Minnesota, 1983.
(13) Keunings, R.; Bousfield D. W. *J. Non-Newtonian Fluid Mech.* **1987**, *22*, 219.
(14) Brandrup, J.; Immergut, E. H. *Polymer Handbook*, 3rd ed.; John Wiley: New York, 1989.
(15) Fox, T. G.; Gratch, S.; Loshaek, S. In *Rheology*; Eirich, F. R., Ed.; Academic Press: New York, 1956; Vol. 1, Chapter 12.
(16) Sperling, L. H. *Introduction to Physical Polymer Science*; Wiley & Sons: New York, 1986.
(17) Nix, W. D.; Gao, H. *J. Mech. Phys. Solids* **1998**, *46*, 411.
(18) Callister, W. D. *Materials Science and Engineering: An Introduction*, 3rd ed.; Wiley & Sons: New York, 1994.
(19) Kajiyama, T.; Tanaka, K.; Takahara, A. *Macromolecules* **1997**, *30*, 280.
(20) Strojny, A. S.; Xia, X.; Tsou, A.; Gerberich, W. W. *J. Adhes. Sci. Technol.* **1998**, *12*, 1299.
(21) Evans, D. F.; Wennerström, A. *The Colloidal Domain*; VCH Publishers: New York, 1994.

MA001762H